Received: 16 May 2017 | Revised: 18 August 2017 | Accepted: 31 August 2017

DOI: 10.1002/eqe.2982

RESEARCH ARTICLE

WILEY

Dynamic buckling of braces in concentrically braced frames

Sina Kazemzadeh Azad | Cem Topkaya | Milad Bybordiani

Department of Civil Engineering, Middle East Technical University, Ankara, Turkey

Correspondence
Cem Topkaya, Department of Civil Engineering, Middle East Technical University, Ankara, Turkey.
Email: ctopkaya@metu.edu.tr

Abstract

Axially loaded members might experience compressive forces above their static buckling capacity because of dynamic buckling under rapid shortening. Although the subject is studied in the context of engineering mechanics, it has not been thoroughly investigated in the field of earthquake engineering. Such dynamic overshoots in the compressive capacity can also be observed for braces of concentrically braced frames (CBFs) during earthquakes. Consequently, a comprehensive investigation is conducted in this study regarding the effects of dynamic buckling of braces on the seismic behavior of steel CBFs. After providing a theoretical background, recent dynamic experiments on braces and CBFs are simulated and discussed to investigate the occurrence of dynamic overshoot during these tests. Eight archetype CBFs are then designed, modeled, and subjected to a large set of ground motions to provide a quantified insight on the frequency and anticipated level of dynamic overshoot in the compressive capacity of braces during earthquakes. Results of a total of 1600 nonlinear time history analyses revealed that dynamic overshoots occur frequently in braces and affect the behavior of CBFs notably. Considerable increases are recorded in forces transmitted to other members of CBFs as a consequence of such dynamic overshoots. Importance of incorporating these dynamic overshoots in the capacity design procedure of columns, beams, and gusset plates is highlighted. Furthermore, results of a parametric study are presented and summarized in the form of a simple formula that can be used as a guide for estimating the level of dynamic overshoot.

KEYWORDS

concentrically braced frames, dynamic buckling, loading rate, nonlinear time history analysis, seismic behavior, steel

1 | INTRODUCTION

Stability of members under *static* and *dynamic* loading conditions has been studied in the past.[1-3] Studies on dynamic stability of compression elements such as columns and rods can be broadly categorized into 2 main subcategories[3]: parametric resonance and stability under impulsive actions. A rod might experience parametric resonance when it is subjected to a harmonic axial force with an oscillation frequency that has a certain relation to the natural frequency of the member.[3-7] The second subclass is concerned with the stability of compression members under impulsive actions such as the impact of a mass, a rapidly applied axial force, or an imposed boundary velocity.[8-20] A brief summary of these studies, which are mostly conducted prior to the 1980s, can be found in Galambos[3] and Simitses,[21] while more recent

studies in this active field of research can be found in Hao et al, Ji and Waas, Mimura et al, Motamarri and Suryanarayan, Morozov et al, and Kuzkin and Dannert.[22-28] The common consensus in the above studies is that, under impulsive actions, the axial force of a member can easily exceed its static critical load.

External impulsive actions that can cause axial strain rates of the order of 10^{-1} to 10^{2} s^{-1} in a rod are generally considered as *low-velocity excitations* while actions with a resulting axial strain rate of 10^{2} to 10^{6} s^{-1} as *high-velocity excitations*.[3] Investigation of high-velocity excitations, which are typically encountered under impact or blast conditions, is out of the scope of the current study. Previous studies[9,13,19,26,29-32] have shown that, in low-velocity excitations with low to moderate compression speeds, the expected buckled shape is identical to the fundamental buckling mode observed in a quasi-static case; however, for high compression speeds, higher buckling modes might also be excited.

During strong ground motions, brace members in steel concentrically braced frames (CBFs) exhibit rapid shortenings and elongations leading to repeated cycles of buckling in compression and yielding in tension. When a rod is subjected to rapid shortening, due to the inertia effect of the rod's mass, it will take a certain amount of time for the member to deflect laterally and buckle, and within this time period, the axial force of the rod can exceed its Euler load significantly.[9] Similarly, it is possible for braces of a CBF to exhibit loads above their static buckling load (ie, to experience *dynamic overshoot*). Previous experimental and analytical results[9,25,26,28,32] have shown that such dynamic overshoots can range from a few percent to hundreds of times the Euler buckling load. In a brief study by Tada and Suito,[33] it was also demonstrated that the buckling and postbuckling behaviors of truss structures could notably differ under dynamic and static analysis. It is worth noting that the study was, however, conducted considering monotonic loads and rather low compressions speeds (<15 mm/s).

Dynamic buckling behavior of compression members has been mostly studied within the context of engineering mechanics, and there has not been any study focusing on the effects of dynamic buckling of braces on the seismic performance of CBFs. Consequently, the current study investigates in detail the following issues: (i) the frequency that braces of CBFs might experience loads above their static buckling load during strong earthquakes; (ii) the expected level of these dynamic overshoots and their effects on the seismic behavior of CBFs; (iii) possible increases in loads transmitted to other members of the systems because of dynamic overshoots and methods for incorporating them in the capacity design procedure; and (iv) appropriate approaches for modeling braces to capture their dynamic buckling behavior accurately.

Pursuant to these goals, dynamic tests conducted on single brace members and single-story CBFs are simulated by using the finite element (FE) method. A series of nonlinear analyses are then conducted on 8 properly designed archetypes subjected to a large set of ground motions. A comprehensive parametric study is also performed to estimate the expected level of dynamic overshoot in CBF braces. The findings and design recommendations are presented herein.

2 | THEORETICAL BACKGROUND

Previous studies have concentrated on the dynamic stability of rods under a suddenly applied constant load or a load with a prescribed regular variation,[8,12,15,27,29,31,34-37] the impact of a mass with a predefined initial velocity,[10,13,16,17,20,23,24] or an imposed constant velocity to one end of the member.[9,25,26,28,32,38,39] Considering the complexity of the loading history that an earthquake typically applies to a brace member, FE analysis is utilized in this paper. Nevertheless, in this section, a simple case of dynamic buckling, initially studied by Hoff,[9] is considered to present a brief theoretical background.

The investigated case is a low-velocity excitation of a simply supported elastic rod with an *effective buckling length* of l under a prescribed boundary velocity where one end of the member moves toward the other end with a constant velocity of v (Figure 1A). Considering the equilibrium of vertical forces in the infinitesimal segment of the rod shown in Figure 1B and taking moments about point o and, finally, applying the moment curvature relation, the differential equation for the deflection of the rod can readily be established as follows[14]:

$$EI\frac{\partial^4(y-y_o)}{\partial x^4}+P\frac{\partial^2 y}{\partial x^2}+\rho A\frac{\partial^2 y}{\partial t^2}=0 \tag{1}$$

where E is the elastic modulus of the material, I is the moment of inertia of the rod's cross section, $y(x,t)$ is the total deflection and $y_o(x)$ is the deflection of the rod due to initial imperfections, $P(t)$ is the axial force in the rod, ρ is the material density, and A is the cross sectional area of the rod. Pure shortening of the rod due to axial straining, that

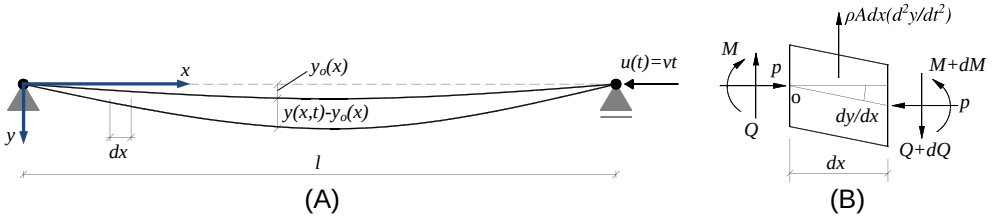

FIGURE 1 Rod under a constant boundary velocity (A) deflected shape and (B) an infinitesimal segment of the rod [Colour figure can be viewed at wileyonlinelibrary.com]

is, $u_a(t)$, is in fact equal to the applied total displacement of $u(t) = vt$ minus the axial displacement due to lateral deflection of the rod, that is, $u_b(t)$. Considering small rotations, $u_b(t)$ can be obtained as follows:

$$u_b(t) = \frac{1}{2}\int_0^l \left[\left(\frac{\partial y}{\partial x}\right)^2 - \left(\frac{\partial y_o}{\partial x}\right)^2\right] dx \tag{2}$$

Consequently, the axial force in the rod can be determined as

$$P(t) = \frac{EA}{l}u_a \;\Rightarrow\; P(t) = \frac{EA}{l}\left(vt - \frac{1}{2}\int_0^l \left[\left(\frac{\partial y}{\partial x}\right)^2 - \left(\frac{\partial y_o}{\partial x}\right)^2\right] dx\right) \tag{3}$$

As mentioned earlier, for low-velocity excitations with low-to-moderate compression speeds, the expected buckled shape is typically identical to the fundamental buckling mode observed in a quasi-static test. Therefore, Hoff[9] approximated the deflected shape of the rod as a half-sine wave, which satisfies the boundary conditions of zero displacement and zero moment at $x = 0$ and $x = l$; that is, $y(x,\tau) = r\, y_m \sin(\pi x/l)$, where r is the radius of gyration of the rod's cross section (ie, $\sqrt{I/A}$), $y_m(\tau)$ is the dimensionless deflection parameter, and thus, ry_m is the maximum lateral deflection of the rod at its mid-span at the investigated time instance, and τ is the dimensionless time defined as $\tau = vtl/\pi^2 r^2$. Similarly, the initial imperfect shape of the rod can be represented as $y_o(x) = r\,\delta\sin(\pi x/l)$, where δ is the dimensionless imperfection parameter, and therefore, $r\delta$ shows the maximum magnitude of initial imperfection of the rod. Substituting $y(x,\tau)$ and $y_o(x)$ in Equations 1 and 3 yields

$$\ddot{y}_m + \Omega\left[\frac{1}{4}y_m^3 + \left(1 - \tau - \frac{\delta^2}{4}\right)y_m - \delta\right] = 0, \quad \text{with } y_m(0) = \delta \text{ and } \dot{y}_m(0) = 0 \tag{4}$$

as well as

$$P(\tau) = P_{cr}\left[\tau - \frac{1}{4}\left(y_m^2 - \delta^2\right)\right] \tag{5}$$

where a dot represents the derivative with respect to τ; P_{cr} is the critical buckling load for a quasi-static case, which is equal to $\pi^2 EI/l^2$ for the considered elastic rod; and Ω is the *dynamic similarity number* introduced by Hoff[9] as

$$\Omega = \frac{\pi^8 c^2}{v^2\lambda^6} \tag{6}$$

where c is the axial velocity of the stress waves in rod's medium (ie, $\sqrt{E/\rho}$) and λ is the slenderness of the rod (ie, l/r). First, the ordinary differential equation presented in Equation 4 should be numerically solved to obtain y_m, and then, using Equation 5, it is possible to capture the variation of axial load during a dynamic buckling.

To demonstrate the issue more clearly, consider the hollow structural section HSS 4 × 4 × 1/8 with a length of 4805 mm, which corresponds to $\lambda \approx 120$, under an applied constant boundary velocity. The Young's modulus of the elastic medium is considered as 200 GPa and its density as 7850 kg/m^3. The maximum magnitude of initial imperfection of the rod is assumed to be $l/1000$. Considering different boundary velocities, Equation 4 was solved by utilizing a Runge-Kutta approach, and the results are summarized in Figure 2. The theoretical results depicted in this figure clearly show that increasing the compression speed (rate) can lead to significant dynamic overshoots in the buckling load of an elastic rod. The FE results presented in the figure will be discussed later in Section 4.

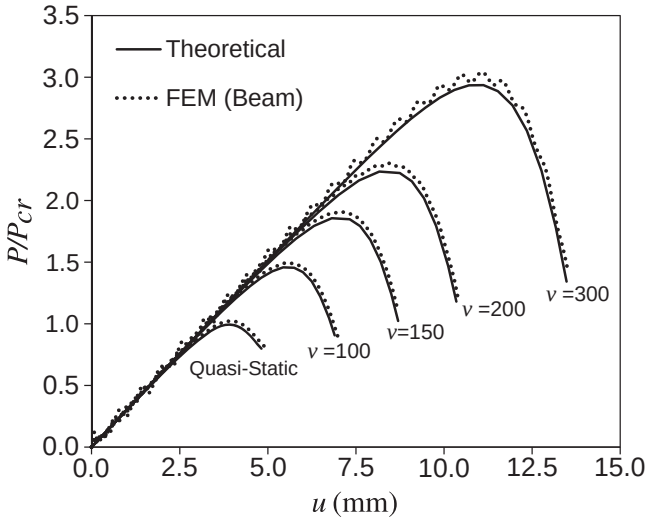

FIGURE 2 Dynamic overshoot in the buckling load of an elastic rod (v in mm/s)

3 | INVESTIGATION OF RECENT DYNAMIC TESTS

The recent dynamic tests conducted on single brace members and single-story CBFs are investigated in this section by FE analysis to observe whether any sign of dynamic overshoot has been reported in these tests under earthquake-level compression rates. All simulations were conducted by using the FE package ABAQUS 6.12-1.[40] It is important to note that, in all FE analyses of this section as well as Sections 4 and 5, the effect of strain rate on changing the strength of steel material was not incorporated into the models. The reason is to have an isolated investigation on the effects of the mass of CBF braces on their dynamic buckling behavior.

3.1 | Dynamic test of Fell on a brace member

The HSS1-3 specimen experimented by Fell[41] is considered here, which was an HSS 4 × 4 × 1/4 steel brace with an effective buckling length of 2985 mm (ie, $\lambda \approx 77$) tested under a cyclic protocol. Details of the specimen are schematically depicted in Figure 3 along with the developed FE model. Following Fell's[41] modeling approach and to reduce the computation time, only a quarter of the specimen was modeled. The boundary conditions depicted in Figure 3B were considered, and the applied displacement history was accurately extracted from the test data (Figure 4) and exerted to the outer nodes of the gusset plate. Eight-node C3D8R brick elements with reduced number of integration points and hourglass control scheme were used for modeling of the brace and gusset plate. Parameters of the utilized von Mises plasticity constitutive model with combined nonlinear isotropic and kinematic hardening were calibrated based on the data provided by Fell.[41] Damping-related information was not reported in Fell and Fell et al,[41,42] and therefore, a small mass proportional damping corresponding to a damping ratio (ξ) of 2.5% in the first mode of vibration was assigned to the FE model. Because the effect of local imperfections was reported by Fell[41] to be negligible, only global imperfections were incorporated in the FE model by using the fundamental buckling mode shape with a maximum amount of $l/1000$.

HSS1-3 was experimented dynamically under a cyclic displacement protocol, with a varying rate, yielding a peak excursion rate (v_{max}) of about 150 mm/s. This rate was selected as a representative speed, which a typical CBF brace member might experience during an earthquake. An identical specimen (HSS1-1) was also tested, however, quasi-statically. The difference between the recorded buckling loads for specimens HSS1-1 and HSS1-3 was reported by Fell[41] to be less than 3%.

It was essential to investigate the reasons for observing no dynamic overshoots in the buckling load of the specimens tested by Fell.[41] The deformed shape of the brace as well as the corresponding von Mises stress contour at the end of the FE analysis are depicted in Figure 3C. The brace axial force (P_{br}) versus brace elongation (u_{br}) response of HSS1-3 reported in the experiment and found here via FE analysis (designated as "FEM [solid]") are presented in Figure 5A and B, respectively. It is worth noting that, during the experiment, the brace force was accurately determined from load cell readings of the utilized actuators.[41] A great level of conformity is observed between the results, which validates the

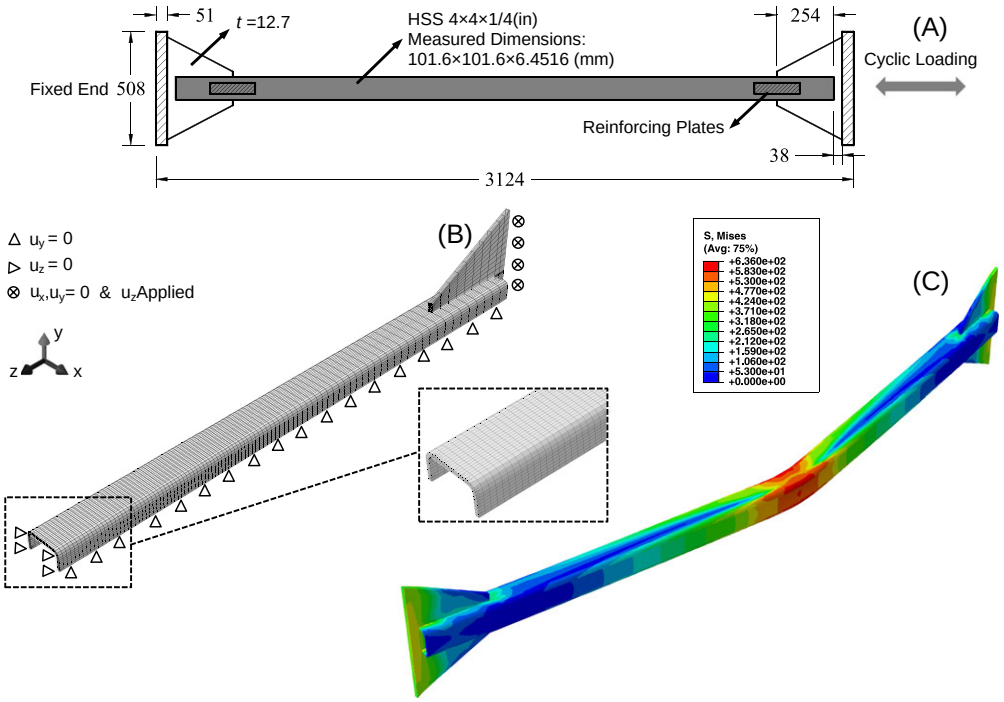

FIGURE 3 Finite element (FE) model of Fell's[41] HSS1-3 test (A) specimen details with dimensions in mm, (B) meshed quarter model, and (C) von Mises stress contour in MPa at the end of the analysis [Colour figure can be viewed at wileyonlinelibrary.com]

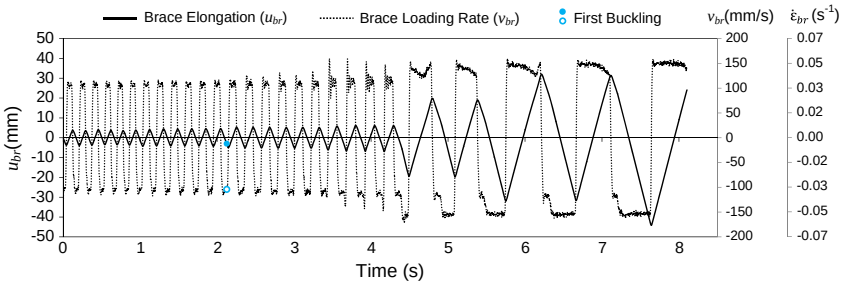

FIGURE 4 Loading history in the HSS1-3 test of Fell[41] (data courtesy of BV Fell); tension (+) compression (−) [Colour figure can be viewed at wileyonlinelibrary.com]

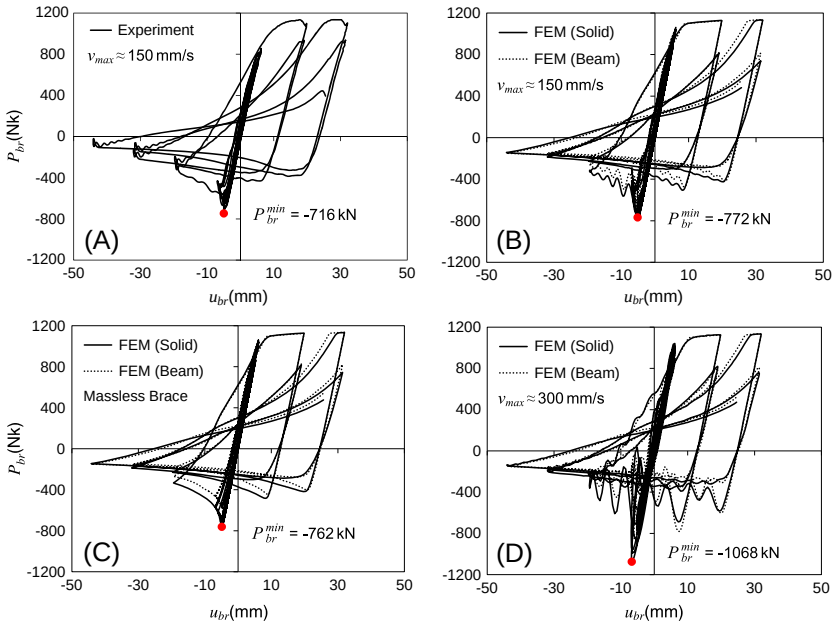

FIGURE 5 Fell's[41] HSS1-3 test results (data courtesy of BV Fell) versus finite element (FE) results of the present study [Colour figure can be viewed at wileyonlinelibrary.com]

FE modeling approach. As reported in these figures, the recorded buckling loads are very similar, with the FE results being slightly higher.

As discussed earlier, mass is the essential parameter in dynamic overshoot, and analyzing a massless brace model will eliminate the possibility of such behavior. Thus, to quantify the level of dynamic overshoot in the buckling load of the HSS1-3 specimen, the simulation was reconducted, this time, with a massless brace; that is, assuming $\rho = 0$. Comparison of the buckling loads reported in Figure 5B and C clearly shows that, although the HSS1-3 test was done with a rather high speed, the specimen did not experience any notable dynamic overshoots.

Variation of *brace loading rate* (v_{br}) for HSS1-3 is depicted in Figure 4 by a dotted line. In this figure, the *brace axial strain rate* ($\dot{\varepsilon}_{br}$) values corresponding to the brace loading rates are also presented in the right vertical axis by dividing the rates by the brace length. Although the loading rate (v_{br}) has the direct effect on the dynamic buckling behavior, the corresponding strain rate ($\dot{\varepsilon}_{br}$) is also reported because it is a normalized quantity that has also been used by others in the context of earthquake engineering.[43] As shown in Figure 4, the peak value of brace loading rate for HSS1-3 was about $v_{max} \approx 150$ mm/s. While being a reasonable estimate, the peak rate reported by Okazaki et al[43] in a recent shake table test for a CBF with comparable brace members demonstrated that such braces might experience significantly higher loading rates. Consequently, it was decided to reanalyze the FE model of the HSS1-3 specimen with twice the previous loading rate (ie, $v_{max} \approx 300$ mm/s), creating a peak strain rate of about 0.10 s^{-1}. The original displacement history (Figure 4) was applied, however, within half of the previous duration. Results for this case, presented in Figure 5D, suggest that the HSS1-3 specimen would have exhibited significant dynamic overshoots in its buckling load, provided that it had been tested with a higher speed. An increase of about 40% is observed in the peak buckling load of the specimen, approaching almost to the yield strength of the brace.

As depicted in Figure 4, during the HSS1-3 test, the brace experienced its first buckling in an early cycle, during a rather small excursion, with a compression rate of about 100 mm/s (<peak value of 150 mm/s) followed by a series of subsequent bucklings prior to the initiation of larger and faster cycles. To further investigate the behavior, the validated FE model was reanalyzed considering a modified displacement protocol that contained a number of small elastic cycles that did not cause buckling in the brace until larger cycles with $u_{br} = \pm 35$ mm and $v_{br} \approx 150$ mm/s initiated. The simulation results, not presented here for brevity, demonstrated that HSS1-3 could have experienced an increase of about 20% in its peak buckling load if it had been experimented with the original loading speed however under such a modified protocol. The results revealed that the overshoot will be more notable particularly if a brace is tested under displacement histories which guarantee buckling during relatively large and fast excursions rather than during small cycles.

3.2 | Shake table test of Goggins on a single-story concentrically braced frame

A number of shake table tests were conducted by Goggins[44] in 2004 on a single-story one-bay by one-bay CBF to study the cyclic behavior of cold-formed steel tubular braces during seismic events. Results of these tests were also summarized and further discussed by Elghazouli et al[45] and Broderick et al.[46] The ST4 test is considered here where the frame was subjected to a sine ramp base acceleration. The input excitation was applied with a constant frequency and an increasing amplitude toward 1.0 g. Details of the specimen as well as the corresponding FE model, developed in the course of this study, are shown in Figure 6. A pair of cold-formed square hollow sections with nominal dimensions of $20 \times 20 \times 2.0$ (mm) was selected as bracing members. As shown in Figure 6B, a sufficient distance was considered between the braces along the z-axis to avoid any contact during the test. The clear length of the brace members between the end stiffeners (Figure 6A) is 3050 mm; however, the utilized connection detail created a rigid end condition for these members, resulting in an effective buckling length of about 1525 mm (ie, $\lambda \approx 200$).

Four-node S4R shell elements with reduced integration, hourglass control mechanism, and 5 through-thickness integration points were used for modeling columns, beams, braces, and their connections. A von Mises plasticity constitutive model with combined nonlinear isotropic and kinematic hardening was utilized for braces, while elastic material was assigned to all other members. Material parameters for the plasticity model were accurately calibrated by using the data reported by Goggins.[44] A mass proportional damping corresponding to $\xi = 3\%$ in the first mode of vibration was assigned to the FE model based on the reported test data.[44] An initial imperfection of 1% of the brace length was considered based on the recommendations of Goggins and his colleagues.[47,48] During the ST4 test, recording of the axial force of the braces started ahead of the tightening of the connection bolts and therefore a pretension of about 5 kN was recorded in these members. To have a more accurate simulation, this pretension was also imposed by applying a temperature load to the braces, prior to the initiation of the main dynamic analysis. The recorded displacement history of the mass was directly applied in the FE model.

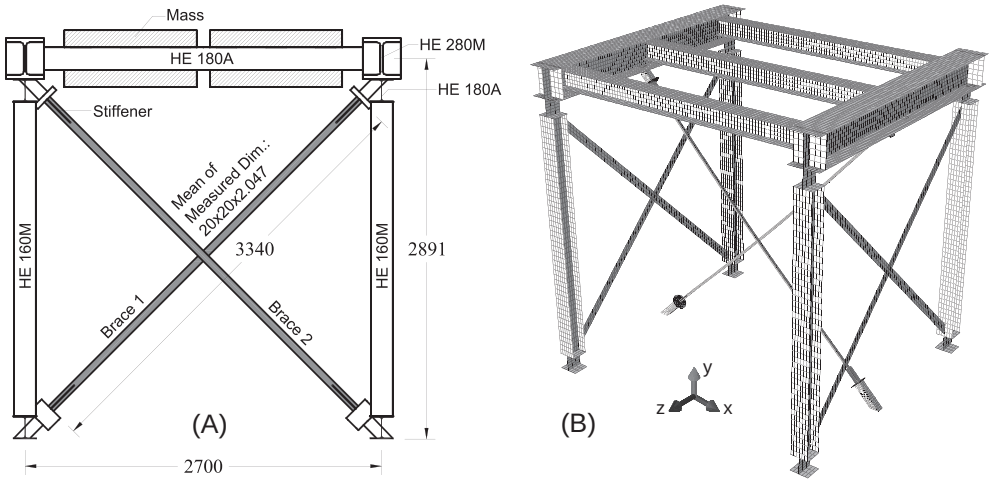

FIGURE 6 Finite element (FE) model of the ST4 test of Goggins[44] (A) specimen details with dimensions in mm and (B) meshed model

A comparison of the test and FE results for Brace 1 is presented in Figure 7A, where the time history of the brace axial force is plotted. During the ST4 test, the axial force of the braces was accurately recorded by connecting their lower ends directly to load cells.[44] Results summarized in Figure 7A demonstrate that the brace behavior was well resembled by the FE analysis. The underestimations observed in peak tensile axial forces are considered to be related to the change of material strength under high strain rates that are not incorporated in the FE model and differences that existed between the assumed and actual material properties and section dimensions. The same issue was also noted in the numerical simulations of Broderick et al.[46]

Significant overshoots above the static buckling capacity of the brace were recorded during the test, which were also captured well by the FE analysis (Figure 7A). For brace loading rates in the range of 120 to 210 mm/s (see the buckling instants in Figure 7C), increases of the order of 100% to 260% were recorded in the compressive capacity of the brace. It is worth noting that the history of u_{br} and v_{br} reported in Figure 7C is based on the FE results for the case of braces with mass. While not addressing the issue comprehensively, Broderick et al[46] found the overshoots in the compressive capacity a topic worthy of attention. For further investigation, the FE model was reanalyzed considering massless

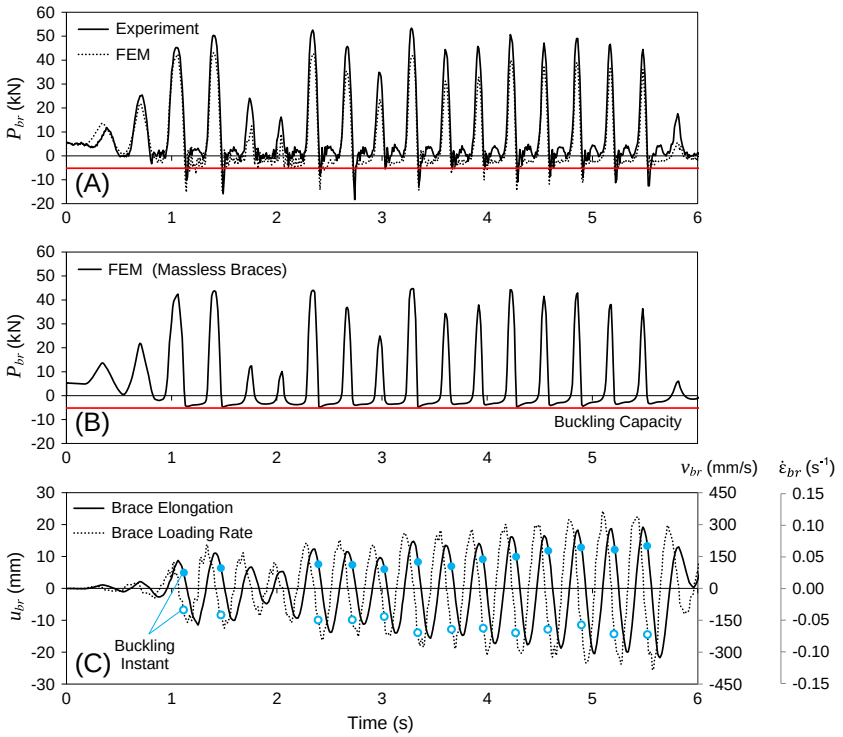

FIGURE 7 Goggins'[44] ST4 test results (data courtesy of S Salawdeh) versus finite element (FE) results of the present study [Colour figure can be viewed at wileyonlinelibrary.com]

braces (ie, assigning $\rho = 0$ only to these members). Comparison of results for this case (Figure 7B) and the original case (Figure 7A) clearly demonstrates that the observed overshoots were solely a consequence of the delaying action of the mass of the brace during dynamic buckling under high compression rates. Furthermore, the results suggest that, in slender braces, such dynamic overshoots can lead to axial forces which drastically exceed the Euler buckling load.

3.3 | Shake table test of Okazaki et al on a single-story concentrically braced frame

A series of shake table tests conducted by Okazaki et al[43] on a single-story one-bay CBF with chevron braces is considered in this section. The frame was subjected to consecutive base excitations with different amplification levels. Here, the focus is on the last test, which had the highest amplification level. A summary of the specimen details as well as the developed FE model are presented in Figure 8. As shown in Figure 8A, the total length of the brace members was 2300 mm; however, the considered elliptic fold lines resulted in an effective buckling length of about 2420 mm (ie, $\lambda \approx 82.5$).

The specimen was modeled by using S4R shell elements (Figure 8B). The displacement of the mass recorded during the experiment was directly applied to the FE model. Due to lack of material data, a von Mises plasticity constitutive model with kinematic hardening considering bilinear material behavior was used in the FE analysis, which was calibrated based on the yield stress, ultimate stress, and elongation values reported by Okazaki et al.[43] Following the recommendation of Okazaki et al,[43] a mass proportional damping corresponding to $\xi = 3\%$ in the first mode of vibration was assigned to the FE model. A residual out-of-plane deformation of 17 mm (ie, $l/133$) was considered based on the reported value for Brace 1 prior to the last test.

Comparison of the experiment results with those of the FE analysis is presented in Figure 9. As shown in Figure 9A, the frame response in base shear (V_b) versus interstory drift ratio (Δ) is accurately captured by the simulation. A reasonable level of conformity is also observed in Figure 9B, which compares the response of Brace 1 during the test and FE analysis. As discussed by Okazaki et al,[43] the brace forces for the experiment were backcalculated by using strain gauge readings combined with an assumed equilibrium condition, and thus, high precision should not be expected for these forces. Nevertheless, the utilized technique in this test was also conceptually capable of recording dynamic and inertia-induced effects in brace forces.

No notable sign of dynamic overshoot was observed in the experiment or FE results. This can be attributed to the considered high level of initial imperfection ($l/133$) for a brace with $\lambda \approx 82.5$. To substantiate this claim, the initial

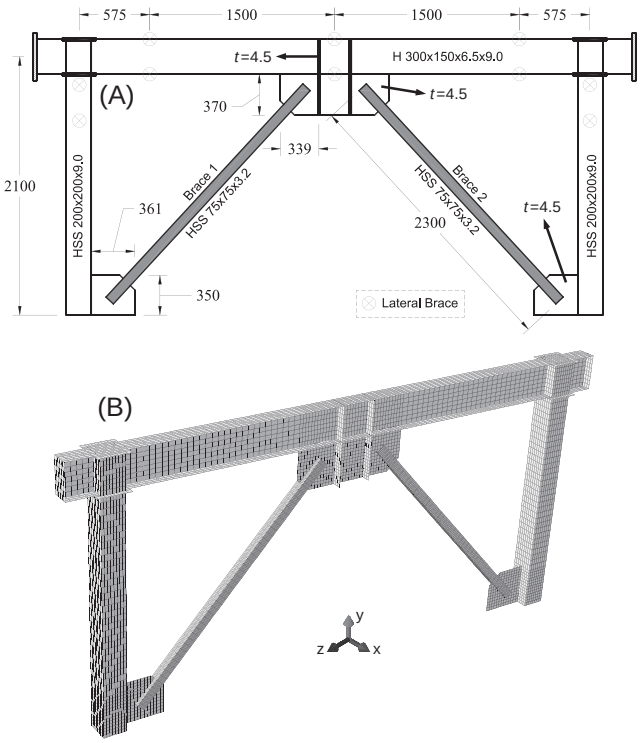

FIGURE 8 Finite element (FE) model of Okazaki et al's[43] test (A) specimen details with dimensions in mm and (B) meshed model

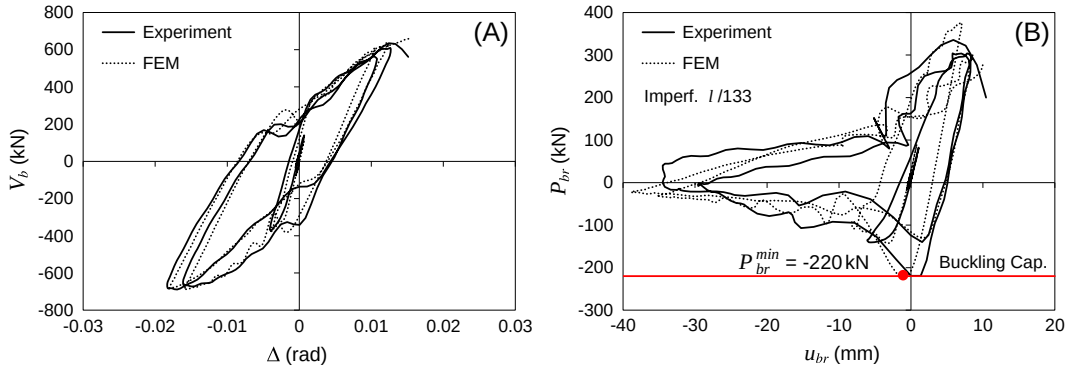

FIGURE 9 Okazaki et al's[43] test results (data courtesy of T Okazaki) versus finite element (FE) results of the present study [Colour figure can be viewed at wileyonlinelibrary.com]

imperfection in the FE model was reduced to a more reasonable level (ie, $l/1000$) and the analysis was reconducted 2 times: that is, considering braces with mass and without mass. Comparison of the results presented in Figure 10A with those of Figure 10B reveals that, if the frame with virgin brace specimens was directly subjected to the highest amplification level, dynamic overshoots of the order of 15% would have been observed in the buckling load of the braces.

Time history of u_{br} and v_{br}, extracted from the FE results, is reported in Figure 10C. Considering the blue symbols in Figure 10C, it can be observed that the loading rates corresponding to buckling instants are much lower than the peak values of v_{br}. In other words, although rather high loading rates were recorded, buckling of the brace happened generally at $v_{br} \approx 200$ mm/s. Results of a supplementary FE analysis, in which the same displacement history was applied within half of the original duration, demonstrated dynamic overshoots as high as 35% above the static buckling load.

4 | EFFECT OF DYNAMIC BUCKLING OF BRACES ON SEISMIC BEHAVIOR OF CONCENTRICALLY BRACED FRAMES

The results presented in Section 3 demonstrated that dynamic overshoot in the compressive capacity of brace members is either reported in some of the recent experimental studies or it would have been readily observed provided that the

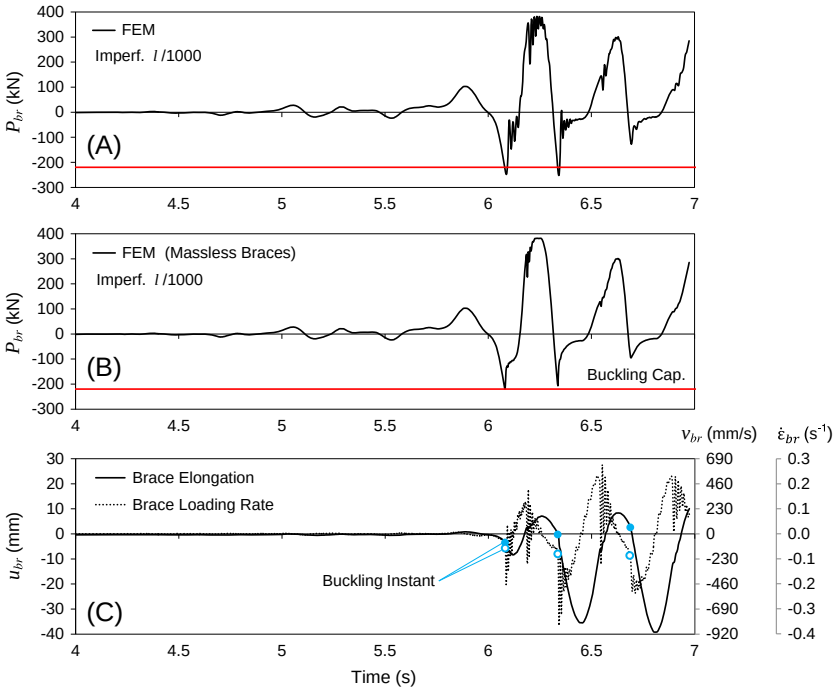

FIGURE 10 Finite element (FE) results of reanalyzing the shake table test of Okazaki et al[43] with an initial imperfection of $l/1000$ [Colour figure can be viewed at wileyonlinelibrary.com]

experiment was conducted with slight modifications. Considering the stochastic nature of earthquakes combined with different possibilities of structural configurations, a comprehensive study is undertaken in this section. The aim is to provide a quantified insight on the frequency of occurrence as well as the anticipated level of dynamic overshoot in the compressive capacity of braces during strong seismic events. Furthermore, the effects of such dynamic overshoots on the behavior of CBF systems and their members are investigated.

4.1 | Design and analysis of archetypes

A total of 8 archetype CBF structures were designed considering the plan geometries of the SAC 9-story and SAC 3-story buildings.[49] Plan dimensions and story heights of the buildings as well as the location and designation of the archetype CBFs are summarized in Figure 11. As shown in this figure, X-braced and V-braced frames located at the perimeter of the buildings were considered as the archetype CBFs. For V-braced frames, chevron (inverted V) bracings were utilized and for X-braced frames, conventional X-bracings were assumed for the 3-story CBFs, whereas two-story split X-bracings were considered for the 9-story CBFs. Each archetype was designed 2 times, once as per American (AISC 360-10,[50] AISC 341-10,[51] and ASCE 7-10[52]) and once as per European (Eurocode 3[53] and Eurocode 8[54]) provisions to cover a wide range of systems with various brace slenderness values. The American frames were designed as *Special* CBFs whereas the European frames as *Ductility Class High* CBFs. Beams and columns were selected from American wide flange sections made of ASTM A992 steel with a yield stress of $F_y = 345$ MPa, while HSS made of ASTM A500 Grade B steel ($F_y = 317$ MPa) were considered for braces. For the US designs, the building was assumed to belong to the seismic design category $D_{\max}$, according to FEMA P695,[55] which represents the highest seismic hazard level with $S_{DS} = 1.0$ g and $S_{D1} = 0.6$ g. Accordingly, $a_g = 0.35$ g with Type C ground was considered as the seismic hazard in the European designs.

Selected member sizes for the designed archetype CBFs are presented in Figure 12. The 9-story archetypes were previously designed by Kazemzadeh Azad et al,[56] and the 3-story archetypes were designed by using a similar procedure in the present study. The colored and underlined numbers in the figure represent the brace slenderness (λ) at each story, which ranges from 40 to 150. It should be noted that all of the beam-to-column, brace-to-beam, and brace-to-column connections are pinned. Also, X-bracing members are not connected to each other at their midpoints. As shown in Figure 12, each archetype is designated with a two-parted name where the first part specifies the number of stories as well as the bracing scheme and the second part shows the utilized design provisions. For instance, "9V-US" is a 9-story CBF with chevron bracings designed as per American provisions.

Two-dimensional models of the archetype CBFs were developed in ABAQUS by adopting the modeling and analysis approaches used by Kazemzadeh Azad et al.[56] All members of the frame and the leaner column were modeled by using B21 two-node beam elements, each having 1 integration point at the midlength and 5 integration points through the height of the section. A rather small mesh size was employed with 12, 18, and 8 elements in each brace, beam, and

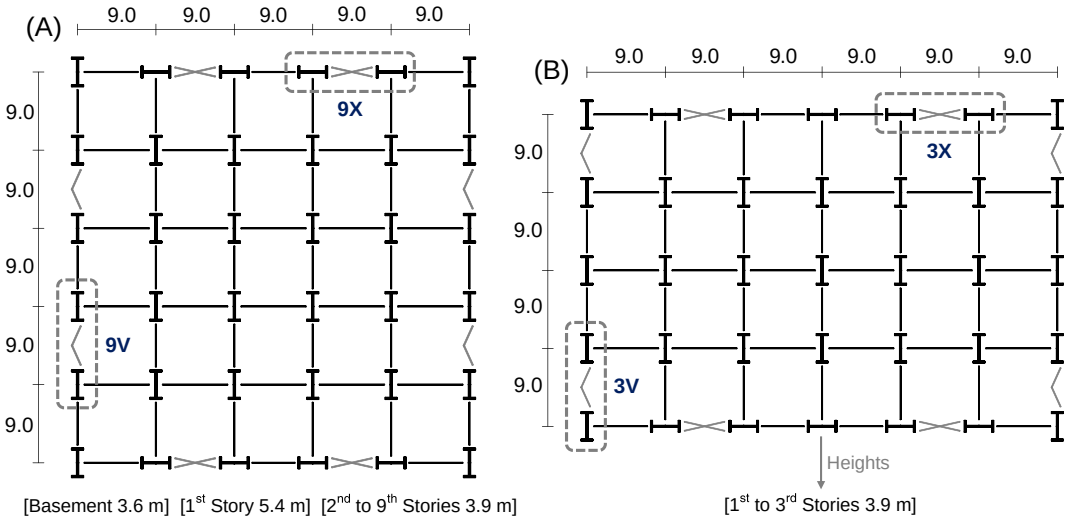

FIGURE 11 Plan dimensions and story heights (in meter) for the archetype buildings (A) 9-story and (B) 3-story [Colour figure can be viewed at wileyonlinelibrary.com]

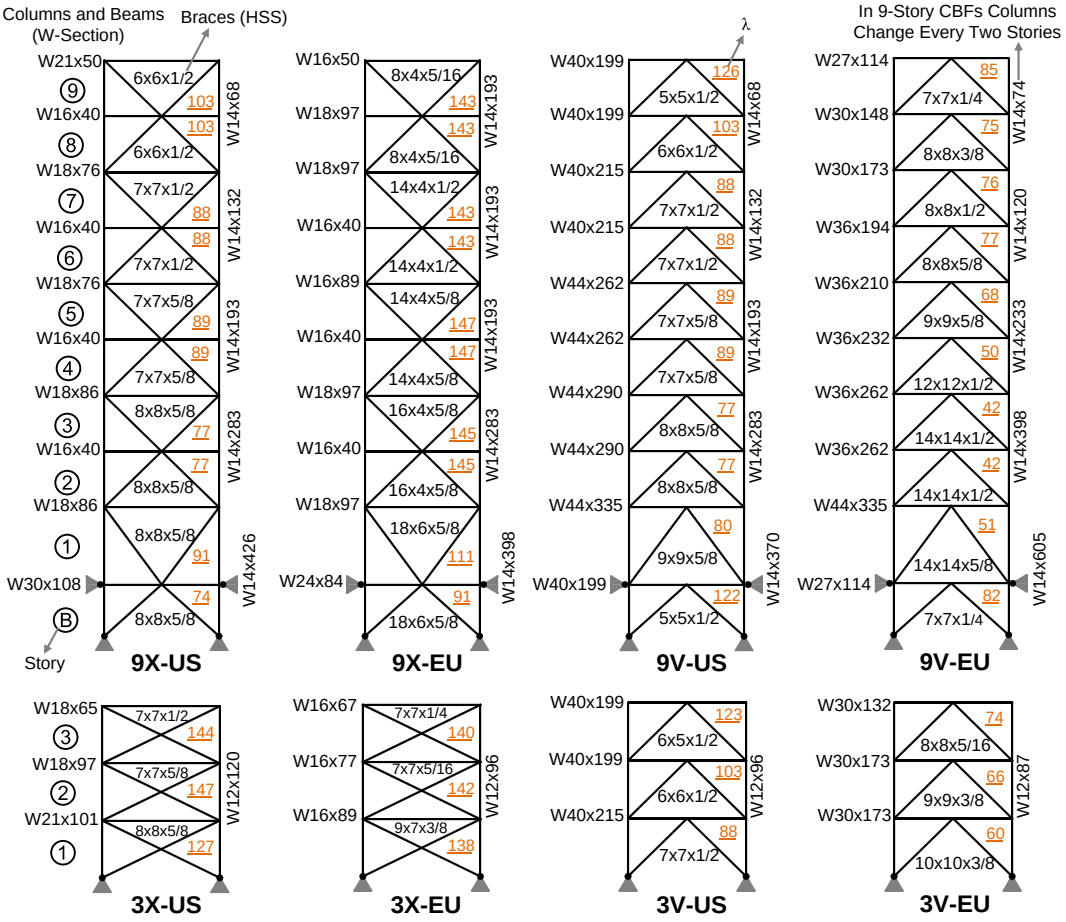

FIGURE 12 Selected member sizes for the designed archetype concentrically braced frames (CBFs) [Colour figure can be viewed at wileyonlinelibrary.com]

column, respectively. For each brace member, an initial imperfection of $l/1000$ was considered. This amount of imperfection has been previously reported as a reasonable estimate by Deierlein et al[57] and also used successfully in numerical simulations of many other studies such as Fell and Okazaki et al.[41,43] Damping corresponding to $\xi = 5\%$ in the first mode of vibration was assigned to each model.

The reliability of beam elements is first validated based on the results of 2 of the previously studied cases. For the first case, the theoretical results obtained in Section 2 and presented in Figure 2 are considered. The same elastic steel rod with $\lambda \approx 120$ was modeled with 12 beam elements and subjected to different boundary velocities. The FE results, depicted in Figure 2 with dotted lines, agree well with the theoretical results. The slight oscillations in the FE results, which are not observed in the theoretical results, are a consequence of the simplifications that were considered in the theoretical solution (eg, neglect of the effect of axial inertia). For the second case, the FE analyses conducted in Section 3 for Fell's[41] HSS1-3 test were repeated, this time using 12 beam elements along the brace length and omitting the gusset plates. The results presented in Figure 5 with dotted lines demonstrate that beam elements are also capable of capturing the behavior of brace members with a reasonable accuracy.

The FE model of each of the 8 archetype CBFs was then subjected to a large set of 44 far-field and 56 near-field ground motion records presented in FEMA P695.[55] Furthermore, each analysis was conducted 2 times, considering braces with mass and massless braces, resulting in a total of 1600 nonlinear time history analyses. It should be emphasized that, in models with braces with mass, in addition to the lumped story masses, the mass of all members, that is, braces, columns, and beams, was included, whereas in the models with massless braces, only the mass of brace members was set to zero and all other masses were retained. The ground motions discussed above were normalized and scaled by using the procedure recommended in FEMA P695[55] to reach the maximum considered earthquake spectral demand of the seismic design category $D_{\max}$.

4.2 | Discussion of results

The results are too voluminous to be presented in every detail. Several local and global performance indicators are compared for the cases of braces with mass and massless braces. As representatives, a summary of results for the 3-story CBFs under near-field records and 9-story CBFs under far-field ground motions is presented in Figures 13 and 14, respectively. In these figures, P_{col}, P_{beam}, P_{br}, μ_{br}, $\delta_{\text{brø}}$, and Δ are the *maximum* values of column axial force, beam axial force, brace axial force, brace ductility demand (ie, brace axial deformation divided by brace axial yield deformation), brace out-of-plane deformation, and interstory drift ratio, respectively, recorded during the analysis. The superscript "*M*" represents the case of braces with mass and "ML" the case with massless braces. Thus, for instance, $P^{M}_{\text{col}}/P^{\text{ML}}_{\text{col}}$ is the amount of change in the maximum recorded column axial force solely due to dynamic buckling of brace members. In each subplot, thin horizontal gray lines span from the minimum to the maximum value of change, thick gray lines cover the mean $\pm$ one standard deviation of change, and circles represent the median of the amount of change recorded for the earthquake set. For P_{col}, P_{beam}, P_{br}, and μ_{br} 2 sets of lines are plotted at each story level to distinguish the amount of change in tension and compression. In general, the difference in results obtained for far-field and near-field records was not very significant regarding the effects of dynamic buckling of braces on the seismic behavior. Reasons for this are discussed later.

It should be emphasized that any change that is recorded in the response due to dynamic buckling of braces is in fact a consequence of 2 issues: (i) increase in the compressive capacity of brace members due to the delaying effect of the mass, that is, dynamic overshoot, and (ii) inertia-induced oscillation in the axial response of brace members. These 2 effects are clearly visible in the results presented previously in Section 3 (Figures 5D, 7A, and 10A). According to these results, the oscillation occurs only after the overshoot phase and within a lower load range compared with the peak buckling load. Thus, the overshoot is the dominant factor, and the above-mentioned 2 effects are briefly referred to as "dynamic overshoot" hereafter.

The third row of subplots in Figures 13 and 14 (ie, $P^{M}_{\text{br}}/P^{\text{ML}}_{\text{br}}$) provides an estimate of the expected level of dynamic overshoot for braces of the studied archetypes. In these subplots, the black circles that lie on the vertical line of $P^{M}_{\text{br}}/P^{\text{ML}}_{\text{br}} = 1.0$ indicate that there is almost no change in the recorded maximum tensile force of brace members, due

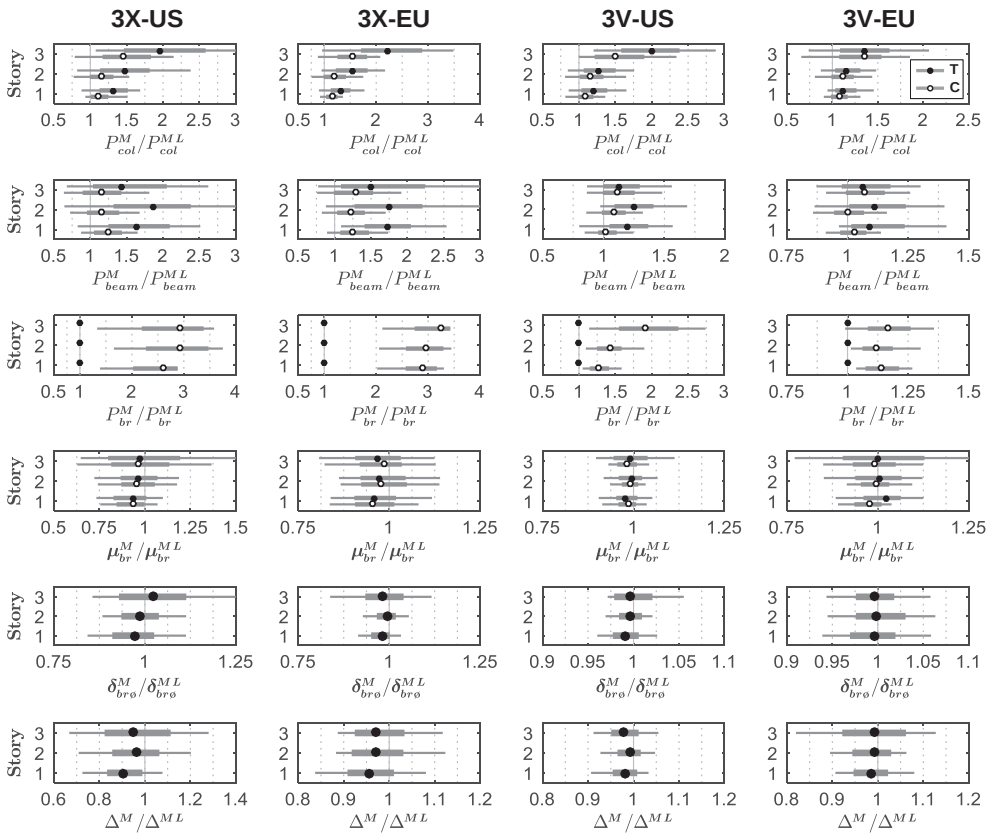

FIGURE 13 Summary of results for 3-story archetype concentrically braced frames (CBFs) under near-field ground motions

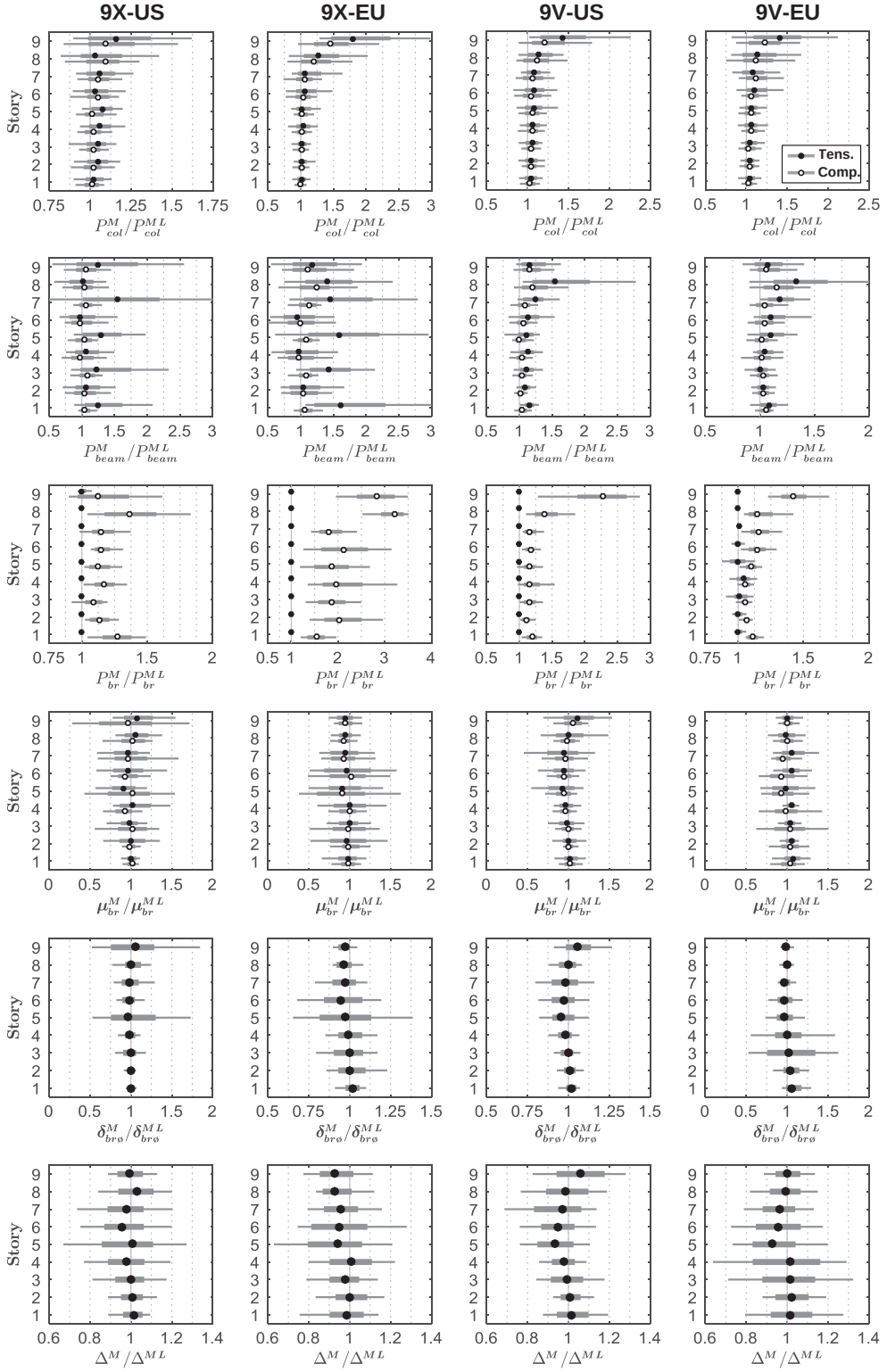

FIGURE 14 Summary of results for 9-story archetype concentrically braced frames (CBFs) under far-field ground motions

to the inclusion of their mass in the analysis models. On the other hand, significant dynamic overshoots are observed in the maximum compressive force of braces, which range from about 10% to very high values of the order of 200%. Investigation of the numerical results revealed that, although the experienced loading rate is also effective, the most dominant parameter regarding the amount of dynamic overshoot is the brace slenderness (λ). The highest levels of overshoots are recorded for 9X-EU, 3X-US, and 3X-EU frames that have the most slender braces (Figure 12).

Although dynamic overshoots do not happen simultaneously for all braces, notable changes in column forces (ie, $P^{M}_{\text{col}}/P^{\text{ML}}_{\text{col}}$) are observed with a general increasing trend toward the upper stories. This is expected because upper columns are less loaded than the lower ones, and thus, dynamic overshoots can result in higher changes in their internal forces. Statistical distribution of the results indicates that, in most cases, column axial forces increased due to dynamic overshoots. The amount of increase varies drastically along the height and among the archetypes, being as high as 20% in lower stories of the 9-story CBFs, ranging to values in excess of 50% in upper stories of these archetypes, and to even higher values in the top story of the 3-story CBFs. The results also indicate that the amount of increase is generally higher for columns connected to more slender braces.

Based on the $P^{M}_{\text{beam}}/P^{\text{ML}}_{\text{beam}}$ subplots, increases in excess of 100% in the tensile axial force and of the order of 25% in the compressive axial force can be observed for beams of 9X-US and 9X-EU frames, located at stories with odd numbers. The reason for the former is that these beams are typically under compression or small tensile forces due to the utilized brace configuration and any increase in their tensile force results in large $P^{M}_{\text{beam}}/P^{\text{ML}}_{\text{beam}}$ ratios. Brace-intersected beams of 9X-US and 9X-EU located at stories with even numbers have mostly experienced similar changes in their tensile and compressive axial forces, within the bounds of ±25% because any change in the exerted unbalanced force will affect the tensile and compressive axial force of these beams somewhat similarly. The abrupt increases in the tensile axial force of beams of 3X-US and 3X-EU are due to the same reason discussed above for beams of 9X-US and 9X-EU located at stories with odd numbers. However, these beams have also mostly experienced significant increases in their compressive axial force, which easily reached to values as high as 50%. For the 9- and 3-story V-braced frames, more uniform height-wise increases in beam axial force are observed, which are mostly bounded by 25% and are found to be higher in tension. The fact that each beam in V-braced archetypes is typically connected to 4 brace members suggests that the tensile axial force of beams would be more affected when the connecting compression braces exhibit dynamic overshoots.

As shown in Figures 13 and 14, both increases and reductions are observed in the brace ductility demands (ie, $\mu^{M}_{\text{br}}/\mu^{\text{ML}}_{\text{br}}$) with a slight tendency toward reduction. The amount of change in μ due to dynamic overshoots is found to be less sensitive to the brace slenderness and mostly bounded by ±25% in the 9-story CBFs and ±10% in the 3-story archetypes. Similarly, the change in brace out-of-plane deformations (ie, $\delta^{M}_{br\text{ø}}/\delta^{\text{ML}}_{br\text{ø}}$), is also less sensitive to the brace slenderness and mostly stays within the limits of ±10% in the 9-story systems and ±5% in the 3-story CBFs. Furthermore, because of overshoots, changes in the range of ±10% are recorded for the maximum interstory drift ratios (ie, $\Delta^{M}/\Delta^{\text{ML}}$) with a notably higher tendency toward reducing the amount of drifts observed during the earthquakes.

Recorded maximum base shears for the cases with braces with mass are compared in Figure 15 with those of the cases with massless braces. Considering that the ratios of $V^{M}_{b}/V^{\text{ML}}_{b}$ are mostly above 1.0, it can be deduced that the figure is in fact quantifying the level of *structural overstrength* solely due to dynamic overshoots in brace forces. Higher overstrengths are recorded for the low-rise systems and those with more slender brace members. Very high overstrengths of the order of 50% are recorded in some cases; however, most recorded overstrengths are bounded by 12% in the 9-story archetypes and by 25% in the 3-story CBFs.

4.3 | Further important inferences

The effect of dynamic overshoot is not directly accounted for in the typical design procedure of CBFs outlined in most seismic provisions.[51,54] This indicates that any additional force that is transmitted to other members due to dynamic

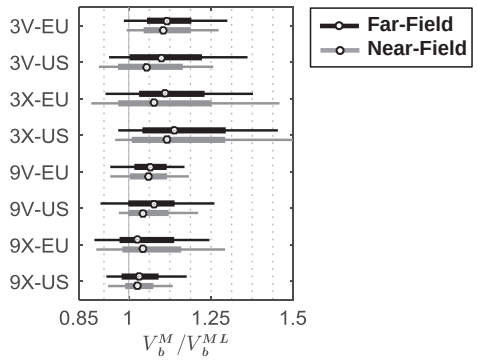

FIGURE 15 Summary of changes recorded for maximum base shears

overshoot in brace forces will be unaccounted for, being more pronounced for designs that utilize more slender brace members. Such additional forces are in many cases too high to be neglected. Consequently, development of methods to account for these additional forces in the *capacity design* procedure of members other than braces seems to be necessary. For instance, the design procedures of Eurocode 8[54] (for all types of CBFs) and AISC 341-10[51] (only for *Ordinary* CBFs) utilize an amplified load approach for the capacity design of columns where the seismic forces in column members are amplified with *structural overstrength factors* (Ω). Such factors can be reevaluated by using data similar to that presented in Figure 15. On the other hand, if the capacity design procedure is based on a plastic collapse mechanism type of analysis (eg, Special CBFs as per AISC 341-10[51]) where braces are replaced by their ultimate tensile (T_{ult}) and compressive (C_{ult}) forces, then measures for including the effect of dynamic overshoot in the ultimate compressive force of braces can be introduced. According to AISC 341-10,[51] the ultimate brace forces can be determined as follows:

$$T_{ult} = R_y F_y A \tag{7}$$

$$C_{ult} = \begin{cases} 1.14\alpha F_{cre} A \le T_{ult} \\ \text{or} \\ 0.3\times(1.14F_{cre} A) \le 0.3T_{ult} \end{cases} \tag{8}$$

where R_y is the ratio of the expected yield stress to the specified minimum yield stress of the brace material, A is the gross area of the brace, and F_{cre} is the critical stress calculated by using the column buckling equations of AISC 360-10[50] considering the expected yield stress. The factor α, which is discussed below, is equal to 1.0 as per AISC 341-10.[51] The expression that yields the higher demand should be used in Equation 8. The ultimate compressive brace force can be altered considering $\alpha \ge 1.0$ to include the dynamic buckling effect. Parameter α is in fact a calibrated *amplification factor* for estimating the expected level of dynamic overshoot. Results of a comprehensive parametric study on α are presented in Section 5.

Most seismic provisions require brace end connections to be designed following a capacity design approach. For instance, AISC 341-10[51] requires brace end connections of Special CBFs to be designed for a tensile load of T_{ult} and a compressive load of $1.1C_{ult}$. As discussed in the commentary of these provisions,[51] a factor of 1.1 has been adopted to alleviate the use of conservative column curve equations. Simulation results of the previous section demonstrated that significant dynamic overshoots, which can range from 10% to 200%, and even more can be observed in the compressive capacity of brace members. The ultimate compressive load for the capacity design of these connections and their elements such as gusset plates, bolts, and welds should also account for the effect of dynamic overshoot. The connections can be designed for a compressive load of $1.1C_{ult}$, however, considering an appropriate $\alpha > 1.0$.

In numerical analyses, removing the mass of a brace will prevent occurrence of any dynamic overshoot in its compressive capacity. Consequently, it is advisable to include the mass of braces in all time history analyses and avoid using models that only include lumped masses at story levels and do not consider the mass of structural members along their lengths. It is worth reiterating that the mass of a brace is the dominant factor in observing dynamic overshoot, whereas the mass of other members (ie, beams and columns) does not have a direct effect on this phenomenon. Phenomenological models that simulate the buckling behavior of brace members through special, calibrated axial force versus axial deformation relations should also be avoided as much as possible. These elements do not need to deflect laterally to exhibit buckling behavior and therefore are unable to capture dynamic overshoot and its associated issues regardless of the inclusion or neglect of their mass.

5 | ESTIMATION OF DYNAMIC OVERSHOOT IN BRACE COMPRESSIVE CAPACITY

While P_{br}^{M}/P_{br}^{ML} ratios are presented in Figures 13 and 14, the amounts of overshoot with respect to the static buckling capacity (ie, $\alpha = P_{br}^{M}/P_{cr}$) are given in Figure 16. It should be emphasized that P_{cr} is determined by conducting separate static FE analyses on single brace members, considering both material and geometric nonlinear effects. The yield limit for each brace member (ie, $\alpha_y = P_y/P_{cr}$, where $P_y = AF_y$) is also depicted in the figure with a red triangle. As it can be seen, significant overshoots above P_{cr} have been recorded, which, in some cases, even approach to the yield strength of the brace. The values of α presented in Figure 16 are those experienced by the brace members and therefore can directly be used as a guide during the capacity design of beams and gusset plates. However, because all brace members

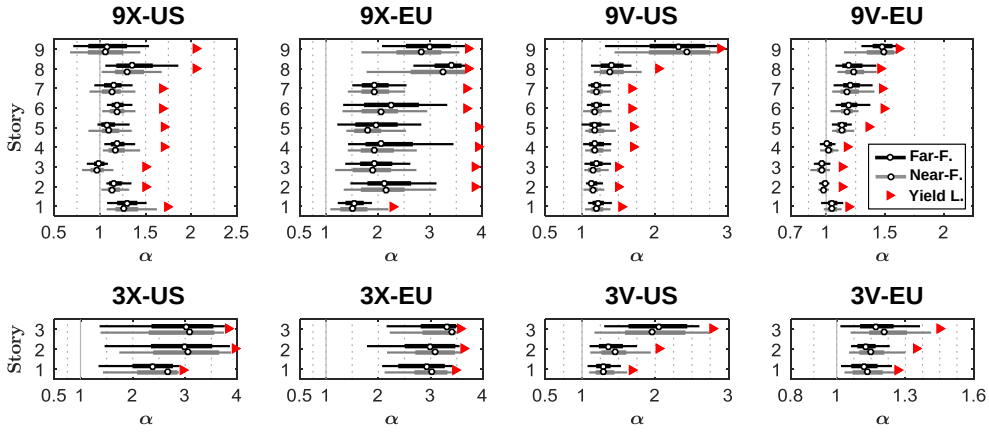

FIGURE 16 Ratio of the recorded maximum compressive brace force divided by the static buckling capacity (ie, α) [Colour figure can be viewed at wileyonlinelibrary.com]

might not exhibit dynamic overshoots simultaneously, more relaxed values of α can be considered for the capacity design of column members.

To provide a more convenient approach for estimating α, another parametric study is conducted in this section. To this end, length of the HSS $4 \times 4 \times 1/4$ brace in the FE model of Fell's[41] HSS1-3 test was altered to obtain 8 different brace models with $\lambda = 40$, 60, 80, 100, 120, 150, 170, and 200. Besides the change in length, the only additional change in the FE model was the omission of gusset plates. Each of the 8 FE models was then subjected to a wide range of compressive loading rates (ie, $v_{br} = 50$ mm/s to 2000 mm/s), where one end of the brace moved toward the other end with a constant speed. Each model was also analyzed once in a quasi-static manner to determine P_{cr}. The applied rates were selected based on the maximum compressive brace loading rates presented in Figure 17, which were extracted from the results of the comprehensive study conducted in Section 4. The figure demonstrates that a typical CBF brace will mostly experience peak loading rates of the order of 250 to 1250 mm/s during strong earthquakes. Higher values of v_{br} were also recorded, particularly in 9X-EU and 9V-EU; however, these are considered to be extreme cases that were observed because of the development of soft story behavior at the top 2 stories of these frames.[56] Based on Figure 17, the recorded maximum brace loading rates during the far-field and near-field earthquakes are comparable, which justifies why the results found in Section 4.2 regarding the effects of dynamic overshoots on seismic behavior were close to each other for these 2 ground motion sets.

A total of 88 refined FE analyses were conducted. As a representative case, results for $\lambda = 60$ are depicted in Figure 18 where dynamic overshoot under rapid shortening is clearly visible. Results for α are summarized in Table 1. Significant overshoots are recorded for high values of v_{br} and particularly for slender braces. The results of this table suggest that, if the compression rate is high enough, yielding prior to notable buckling-induced lateral deformation (ie, *saturation*) might also be observed.

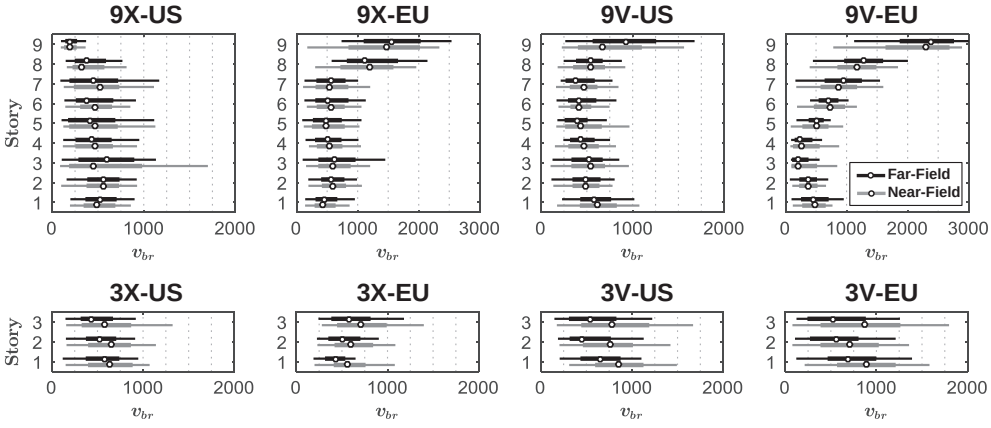

FIGURE 17 Recorded maximum compressive brace loading rates (in mm/s)

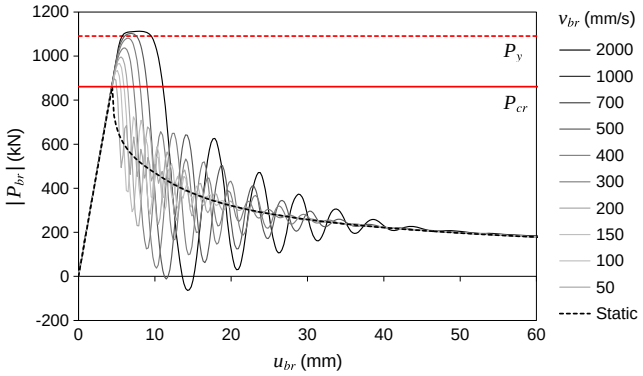

FIGURE 18 Finite element (FE) response of an HSS 4 × 4 × 1/4 steel brace with $\lambda = 60$ to different loading rates [Colour figure can be viewed at wileyonlinelibrary.com]

TABLE 1 Recorded values of α in the parametric study

	v_{br} (mm/s)										
λ	Static	50	100	150	200	300	400	500	700	1000	2000
40	1.00	1.03	1.05	1.07	1.08	Y*	Y	Y	Y	Y	Y
60	1.00	1.04	1.09	1.12	1.16	1.20	1.26	Y	Y	Y	Y
80	1.00	1.06	1.19	1.29	1.40	1.60	1.76	Y	Y	Y	Y
100	1.00	1.08	1.32	1.61	1.87	2.27	2.54	Y	Y	Y	Y
120	1.00	1.21	1.63	2.08	2.49	3.14	3.57	Y	Y	Y	Y
150	1.00	1.50	2.31	3.03	3.69	4.80	5.52	Y	Y	Y	Y
170	1.00	1.82	2.84	3.78	4.63	6.09	7.05	Y	Y	Y	Y
200	1.00	2.30	3.83	4.98	6.14	8.21	9.63	Y	Y	Y	Y

*Indicates that the brace experienced yielding prior to exhibiting notable buckling-induced lateral deformation.

The following issues should be borne in mind regarding the data presented in Table 1. As discussed in Section 3, dynamic overshoot is highly dependent upon the applied displacement history. On the other hand, the results presented in Table 1 are obtained by applying one-sided large compressive excursions with different speeds to the brace. Consequently, the results should be considered as upper bound estimates for α. Another important issue is the applicability of the reported data to other cases. Based on the theoretical background presented in Section 2, it can readily be shown that the amount of overshoot in the buckling load of a pinned elastic brace, with a predefined imperfection, subjected to a boundary velocity is only dependent upon its material, loading rate, and slenderness. Furthermore, results of additional FE analyses, which are not presented here, demonstrated that if material nonlinearity is also included, the overshoot is again dominantly dependent upon the same parameters. In other words, if 2 steel braces of similar slenderness (λ) and imperfection (eg, $l/1000$), one with a section of HSS 4 × 4 × 1/4 and the other with a section of HSS 8 × 8 × 5/6, are subjected to the same loading rate, they will experience similar levels of dynamic overshoot, regardless of the significant difference that exists between their mass per unit length values. This indicates that the overshoot values presented in Table 1 are rather comprehensive and can be used for a variety of steel brace sections with different slenderness values. The main restriction regarding the results is the value of F_y. Based on the material data reported by Fell,[41] the results of Table 1 are for a brace with $F_y \approx 470$ MPa. However, if the material of a steel brace has a higher yield stress, larger overshoots might be observed prior to the saturation of α by the yield limit (ie, α_y). Consequently, the results presented in the table are most reliable for steel braces with $F_y \approx 470$ MPa and can be used as an estimate for those with $F_y < 470$ MPa, however, might be erroneous for cases with $F_y \gg 470$ MPa.

The results reported in Table 1 can be summarized in form of a simple formula to be used as an aid by design engineers. Based on a curve fitting process, the following power law was found to be a reasonable match for the results:

$$\alpha = 1 + \frac{(v_{\mathrm{br}}/c)^{0.85}\,\lambda^{2.5}}{20} \leq \alpha_y \tag{9}$$

Based on the previous discussions, the proposed formula provides an upper bound estimate for the amount of dynamic overshoot that a steel brace ($E = 200$ GPa, $\rho = 7850$ kg/m^3, and $c = \sqrt{E/\rho} \approx 5047$ m/s), with an imperfection of $l/1000$, would experience when subjected to a particular compressive loading rate (v_{br}). The value of overshoot is capped in the formula by the yield limit (α_y). This is in recognition of the saturation of dynamic overshoot and the fact that the increase in the compressive brace force beyond this level was observed to be very limited in the studied FE models and controlled only by the strain hardening behavior of the material. Nevertheless, the threshold of α_y can slightly be altered to also include the strain hardening effect, if required. Other studies such as Motamarri and Suryanarayan and Kuzkin and Dannert[26,28] have also proposed theoretical methods for estimating α, however, only for elastic members. It is worth noting that the mean of ratios of overshoot values found via Equation 9 to those obtained in the FE analyses of this section is 1.02 with a standard deviation of 0.04.

6 | CONCLUSIONS

The dynamic buckling behavior of brace members during strong earthquakes and its effect on the seismic behavior of CBF systems and their members have been thoroughly studied in this paper. The following can be concluded from the study:

- Investigation of the recent dynamic experiments demonstrated that dynamic overshoot in brace forces has been reported, though not discussed thoroughly, in some studies. Furthermore, simulation results revealed that the dynamic overshoot would have been readily observed in other tests provided that the experiment was conducted with slight modifications such as increasing the applied loading rate or altering the utilized displacement history.
- Detailed FE analyses indicated that dynamic buckling of a steel brace is a rather complex phenomenon, which is highly dependent upon many factors such as the brace slenderness, imposed displacement history, magnitude and variation of the loading rate, imperfection of the brace, and the change in its residual out-of-plane deformation.
- Results of a comprehensive study on archetype CBFs revealed that dynamic overshoots can frequently be observed in brace forces during strong earthquakes. Overshoots of the order of 10% to very high values in excess of 200% were recorded in the FE analyses. The brace slenderness as well as the experienced loading rate are the effective factors in the observed level of overshoot, with the former being the most dominant parameter.
- As a consequence of dynamic buckling of braces, notable changes were recorded in forces transmitted to other members of the studied CBF systems. Increases as high as 20% to 150% were recorded in column axial forces for different cases. In general, the percentage of increase is expected to be larger in low-rise CBFs and upper columns of mid- and high-rise CBFs, and more particularly, when slender braces are used in the system. Similarly, considerable increases as high as 25% to 50% were recorded in beam axial forces of the studied archetypes.
- Dynamic buckling of braces was found to be less influential on altering the deformation demands. Changes in brace ductility demands and the maximum interstory drift ratios were mostly bounded by $\pm$25% and $\pm$10%, respectively, with a higher tendency toward reduction due to overshoots.
- Increase in forces transmitted to members other than braces and to brace end connections necessitates revising the current capacity design procedures to include these effects. To this end, structural overstrength factors can be reevaluated by using data similar to that presented in this study, which showed increases as high as 12% to 25% in the recorded maximum base shear, solely due to dynamic overshoots. Furthermore, the presented analysis results and the developed formula (Equation 9) can be used as guides for calibrating amplification factors (α) to be used for proper estimation of ultimate brace forces during capacity design procedures.
- For the studied archetype CBFs, compressive brace loading rates mostly of the order of 250 to 1250 mm/s were recorded during strong earthquakes.
- Omitting the mass of a brace in an analysis model will prevent occurrence of any dynamic overshoot in its compressive capacity. Thus, it is advisable to avoid using analysis models that only include lumped masses at story levels and do not consider the mass of structural members and, more particularly, braces along their lengths. Phenomenological brace models that are unable to capture dynamic overshoot and its associated issues should also be avoided as much as possible in nonlinear time history analyses.

The paper has provided some level of insight on the importance of dynamic buckling of braces on the seismic behavior of CBF systems. However, more research is needed to further elaborate the issue. Additional experiments on

single brace members, utilizing sufficiently high loading rates, would be very fruitful in studying the dynamic overshoots. Shake table tests under strong earthquakes would also be beneficial, particularly if proper means of recording the axial force of brace members can also be used. The most important research need is, however, the development of convenient as well as economic procedures for incorporating the effects of dynamic overshoots in the capacity design of other members of CBFs such as columns, beams, and gusset plates. Although the data presented in this paper provide some guidance on this issue, significant research is still needed to propose design methods, which can be included in the current seismic provisions. Finally, considering the efficiency of phenomenological brace models, special techniques can be developed so that these elements would also be able to mimic dynamic overshoots during rapid shortenings.

ACKNOWLEDGEMENTS

The authors are grateful to Professors Benjamin V Fell, Suhaib Salawdeh, and Taichiro Okazaki for providing the valuable test data presented and discussed in this paper.

ORCID

Sina Kazemzadeh Azad http://orcid.org/0000-0002-2639-0292
Cem Topkaya http://orcid.org/0000-0003-0528-1756

REFERENCES

1. Timoshenko SP, Gere JM. *Theory of Elastic Stability*. 2nd ed. New York: McGraw-Hill; 1961.
2. Bažant ZP, Cedolin L. *Stability of Structures: Elastic, Inelastic, Fracture, and Damage Theories*. New York: Oxford University Press; 1991.
3. Galambos TV. *Guide to Stability Design Criteria for Metal Structures*. 5th ed. New York: John Wiley; 1998.
4. Bolotin VV. *The Dynamic Stability of Elastic Systems*. San Francisco: Holden-Day; 1964.
5. Ibrahim RA. *Parametric Random Vibration*. Letchworth, England: Research Studies Press; 1985.
6. Simitses GJ. *Dynamic Stability of Suddenly Loaded Structures*. New York: Springer-Verlag; 1990.
7. Morozov NF, Tovstik PE. Dynamic loss of stability of a rod under longitudinal load lower than the Eulerian load. *Dokl Phys*. 2013;58(11):510-513.
8. Koning C, Taub J. Impact buckling of thin bars in the elastic range hinged at both ends. National Advisory Committee for Aeronautics, Washington, DC, NACA-TM-748; 1934.
9. Hoff NJ. The dynamics of the buckling of elastic columns. *J. Appl. Mech. ASME*. 1951;18(1):68-74.
10. Gerard G, Becker H. Column behavior under conditions of impact. *J Aeronaut Sci*. 1952;19(1):58-60.
11. Davidson JF. Buckling of struts under dynamic loading. *J Mech Phys Solids*. 1953;2(1):54-66.
12. Huffington NJ. Response of elastic columns to axial pulse loading. *AIAA Journal*. 1963;1(9):2099-2104.
13. Lindberg HE. Impact buckling of a thin bar. *J. Appl. Mech. ASME*. 1965;32(2):315-322.
14. Lindberg HE, Florence AL. *Dynamic Pulse Buckling: Theory and Experiment*. Dordrecht, Netherlands: Springer; 1987.
15. Holzer SM. Stability of columns with transient loads. *J. Eng. Mech. Div. ASCE*. 1970;96(6):913-930.
16. Hayashi T, Sano Y. Dynamic buckling of elastic bars: 1st report, the case of low velocity impact. *Bull JSME*. 1972;15(88):1167-1175.
17. Hayashi T, Sano Y. Dynamic buckling of elastic bars: 2nd report, the case of high velocity impact. *Bull. JSME*. 1972;15(88):1176-1184.
18. Elishakoff I. Axial impact buckling of a column with random initial imperfections. *J. Appl. Mech. ASME*. 1978;45(2):361-365.
19. Lee LHN. Dynamic buckling of an inelastic column. *Int. J. Solids Struct.* 1981;17(3):271-279.
20. Ari-Gur J, Weller T, Singer J. Experimental and theoretical studies of columns under axial impact. *Int. J. Solids Struct.* 1982;18(7):619-641.
21. Simitses GJ. Instability of dynamically loaded structures. *Appl Mech Rev ASME*. 1987;40(10):1403-1408.
22. Hao H, Cheong HK, Cui S. Analysis of imperfect column buckling under intermediate velocity impact. *Int J Solids Struct*. 2000;37(38):5297-5313.
23. Ji W, Waas AM. Dynamic bifurcation buckling of an impacted column. *Int J Eng Sci*. 2008;46(10):958-967.
24. Mimura K, Umeda T, Yu M, Uchida Y, Yaka H. Effects of impact velocity and slenderness ratio on dynamic buckling load for long columns. *Int J Mod Phys B*. 2008;22(31n32):5596-5602.

25. Mimura K, Kikui T, Nishide N, Umeda T, Riku I, Hashimoto H. Buckling behavior of clamped and intermediately supported long rods in the static-dynamic transition velocity region. *J Soc Mat Sci*. 2012;61(11):881-887. (in Japanese)
26. Motamarri P, Suryanarayan S. Unified analytical solution for dynamic elastic buckling of beams for various boundary conditions and loading rates. *Int J Mech Sci*. 2012;56(1):60-69.
27. Morozov NF, Il'in DN, Belyaev AK. Dynamic buckling of a rod under axial jump loading. *Dokl. Phys.* 2013;58(5):191-195.
28. Kuzkin VA, Dannert MM. Buckling of a column under a constant speed compression: a dynamic correction to the Euler formula. *Acta Mech*. 2016;227(6):1645-1652.
29. Housner GW, Tso WK. Dynamic behavior of supercritically loaded struts. *J Eng Mech Div ASCE*. 1962;88(EM5):41-65.
30. Abrahamson GR, Goodier JN. Dynamic flexural buckling of rods within an axial plastic compression wave. *J Appl Mech ASME*. 1966;33(2):241-247.
31. McIvor IK, Bernard JE. The dynamic response of columns under short duration axial loads. *J. Appl. Mech. ASME*. 1973;40(3):688-692.
32. Erickson B, Nardo SV, Patel SA, Hoff NJ. An experimental investigation of the maximum loads supported by elastic columns in rapid compression tests. *Proc Soc Exp Stress Anal*. 1956;14(1):13-20.
33. Tada M, Suito A. Static and dynamic post-buckling behavior of truss structures. *Eng Struct*. 1998;20(4):384-389.
34. Kornev VM. Development of dynamic forms of stability loss of elastic systems under intensive loading over a finite time interval. *J. Appl. Mech. Tech. Phys.* 1972;13(4):536-541.
35. Kornev VM. Asymptotic analysis of the behavior of an elastic bar under aperiodic intensive loading. *J. Appl. Mech. Tech. Phys.* 1972;13(3):398-406.
36. Markin AV. Buckling in an elastic rod under a time-varying load. *J Appl Mech Tech Phys*. 1977;18(1):134-138.
37. Morozov NF, Belyaev AK, Tovstik PE, Tovstik TP. The Ishlinskii-Lavrent'ev problem at the initial stage of motion. *Dokl. Phys.* 2015;60(8):368-371.
38. Sevin E. On the elastic bending of columns due to dynamic axial forces including effects of axial inertia. *J. Appl. Mech. ASME*. 1960;27(1):125-131.
39. Elishakoff I. Hoff's problem in a probabilistic setting. *J. Appl. Mech. ASME*. 1980;47(2):403-408.
40. ABAQUS 6.12-1 [Computer Software]. Providence, RI: Dassault Systèmes, Simulia; 2012.
41. Fell BV. Large-scale testing and simulation of earthquake-induced ultra low cycle fatigue in bracing members subjected to cyclic inelastic buckling. Ph.D. Thesis, Department of Civil and Environmental Engineering, University of California, Davis, CA; 2008.
42. Fell BV, Kanvinde AM, Deierlein GG, Myers AT. Experimental investigation of inelastic cyclic buckling and fracture of steel braces. *J Struct Eng ASCE*. 2009;135(1):19-32.
43. Okazaki T, Lignos DG, Hikino T, Kajiwara K. Dynamic response of a chevron concentrically braced frame. *J. Struct. Eng. ASCE*. 2013;139(4):515-525.
44. Goggins J. Earthquake resistant hollow and filled steel braces. Ph.D. Thesis, Department of Civil, Structural and Environmental Engineering, Trinity College, The University of Dublin, Ireland; 2004.
45. Elghazouli AY, Broderick BM, Goggins J, et al. Shake table testing of tubular steel bracing members. *Struct Build*. 2005;158(4):229-241.
46. Broderick BM, Elghazouli AY, Goggins J. Earthquake testing and response analysis of concentrically-braced sub-frames. *J Constr Steel Res*. 2008;64(9):997-1007.
47. Goggins J, Salawdeh S. Validation of nonlinear time history analysis models for single-storey concentrically braced frames using full-scale shake table tests. *Earthq Eng Struct D*. 2013;42(8):1151-1170.
48. Salawdeh S. Seismic design of concentrically braced steel frames. Ph.D. Thesis, Department of Civil Engineering, National University of Ireland, Galway, Ireland; 2012.
49. FEMA. *State of the Art Report on Systems Performance of Steel Moment Frames Subject to Earthquake Ground Shaking, FEMA-355C*. Washington, DC: SAC Joint Venture, Building Seismic Safety Council for the Federal Emergency Management Agency; 2000.
50. AISC. *Specification for Structural Steel Buildings, ANSI/AISC 360-10*. Chicago, IL: American Institute of Steel Construction; 2010.
51. AISC. *Seismic Provisions for Structural Steel Buildings, ANSI/AISC 341-10*. Chicago, IL: American Institute of Steel Construction; 2010.
52. ASCE. *Minimum Design Loads for Buildings and Other Structures, ASCE/SEI-7-10*. Reston, VA: Structural Engineering Institute of the American Society of Civil Engineers; 2010.
53. Eurocode 3. *Design of Steel Structures—Part 1-1: General Rules and Rules for Buildings, EN 1993-1:2003*. Brussels: European Standard, Comité Européen de Normalisation; 2003.
54. Eurocode 8. *Design of Structures for Earthquake Resistance—Part 1: General Rules, Seismic Actions and Rules for Buildings, EN 1998-1:2004*. Brussels: European Standard, Comité Européen de Normalisation; 2004.
55. FEMA. *Quantification of Building Seismic Performance Factors, FEMA-P695*. Washington, DC: Building Seismic Safety Council for the Federal Emergency Management Agency; 2009.

56. Kazemzadeh Azad S, Topkaya C, Astaneh-Asl A. Seismic behavior of concentrically braced frames designed to AISC341 and EC8 provisions. *J Constr Steel Res*. 2017;133:383-404.

57. Deierlein GG, Reinhord AM, Willford MR. Nonlinear structural analysis for seismic design: a guide for practicing engineers. National Institute of Standards and Technology, Gaithersburg, MD, NIST GCR 10-917-5; 2010.

How to cite this article: Kazemzadeh Azad S, Topkaya C, Bybordiani M. Dynamic buckling of braces in concentrically braced frames. *Earthquake Engng Struct Dyn*. 2017;1–21. https://doi.org/10.1002/eqe.2982